УДК 519.254:517.98

ON STANDARD AND NONSTANDARD APPLICATIONS OF WAVELET ANALYSIS

M.V.Altaisky

We review the present status of wavelet analysis, the method of decomposition with respect to representations of the affine group, which is effectively used everywhere in signal and image processing and is receiving a lot of interest in the context of nuclear physics data analysis. Some results of the application of the wavelet decomposition to the experiments carried out at JINR are presented, and some new possible applications are indicated.

The investigation has been performed at the Laboratory of Nuclear Problems, JINR.

О стандартных и нестандартных приложениях вейлет-анализа

М.В.Алтайский

Вейлет-анализ — метод обработки сигналов и изображений — рассматривается как метод разложений по представлениям аффинной группы. Представлены результаты применения вейлет-анализа к экспериментам, проводимым в ОИЯИ, и возможности некоторых новых приложений.

Работа выполнена в Лаборатории ядерных проблем ОИЯИ.

1. Wavelets: An Intuitive Description of the Method

The principal shortcoming of common Fourier analysis is its nonlocality. Due to the uncertainty principle, a signal cannot be localized simultaneously in frequency and time with arbitrary precession. From the practical standpoint this nonlocality is always undesirable. This means that we usually want (*i*) to keep the contribution of low and high frequencies separately reasonable and (*ii*) we want the decomposition of a signal to be robust with respect to small perturbation; both are evidently not the case for the Fourier decomposition

$$\hat{f}(\omega) = \frac{1}{\sqrt{2\pi}} \int_{-\infty}^{\infty} e^{i\omega x} f(x)\, dx. \tag{1}$$

To overcome this difficulty the *windowed Fourier transform* [1]

$$\hat{f}(\omega, \tau) = \int_{-\infty}^{\infty} e^{i\omega x} f(x)\, \overline{W}(x-\tau)\, dx \tag{2}$$

was suggested by D.Gabor in 1946 for the purposes of signal processing. Unfortunately, there are some faults with this idea. Transform (2) is evidently poor in resolving wavelengths longer than the window $W(x)$ width. Conversely, the decomposition of short, but high frequency signals requires a broad window with a large number of cycles. The process of reconstruction in this case contains a large number of terms with comparable amplitudes and hence turns out to be numerically unstable.

Conspicuously, what one needs is a scheme with a broad window for low frequency signals and a narrow window for high frequency signals. Such a scheme, independently developed by several authors at the beginning of 1980s [2], is called a wavelet transform. Practically, it is a separate convolution of the signal in question with a family of functions obtained from some basic one — basic wavelet — by shifts and dilatations:

$$T_\psi(a,\tau)f=\int_{-\infty}^{\infty}\overline{\psi}_{a,\tau}(x)f(x)\,dx, \tag{3}$$

where

$$\psi_{a,\tau}(x)=\frac{1}{\sqrt{a}}\psi\left(\frac{\tau-x}{a}\right)$$

are usually referred to as (*affine*) *wavelets*.

2. Mathematical Background

Being a quasi-local integral transform, affine wavelet decomposition (3) has found a lot of practical applications to signal processing. In parallel with practical development it has found a profound and abstract theoretical background in the Lie group theory [3]. In the present paper we start with its general properties and only then turn to applications and implementation.

Let us consider a Hilbert space $\mathcal{H}$ with transitive action of a Lie group G on it. Let U be a continuous square-integrable unitary representation of G. The vector $\psi\in\mathcal{H}$ is said to be admissible (with respect to G), if

$$\int_G |\langle\psi, U(g)\,\psi\rangle|^2\,d\mu_L(g)<\infty,$$

where $d\mu_L(g)$ is a left-invariant measure on G.

The key result which allows decomposition of an arbitrary vector $v\in\mathcal{H}$ with respect to the representation $U(g)$, $g\in G$, is summarized by the following theorem[1] [4].

Theorem 1. *Let U be a square-integrable unitary representation of a separable locally compact group G (with left Haar measure $d\mu_L$) on the Hilbert space $\mathcal{H}$, and let $\psi\in\mathcal{H}$ be an admissible vector. Let*

$$C_\psi=\|\psi\|^{-2}\int_G |\langle\psi, U(g)\,\psi\rangle|^2\,d\mu_L(g)<\infty \tag{4}$$

($\|\cdot\|$ *– L^2-norm is implied*).

[1]Here we present the weak form of the theorem. In general, the unitarity is not strictly required.

Then for all $v \in \mathcal{H}$ the following decomposition holds (the integrals converging weakly)

$$v = C_\psi^{-1} \int_G \langle v, U(g)\,\psi\rangle\, U(g)\,\psi d\mu_L(g). \tag{5}$$

Thus, to acquire good analytical properties, we must require the window integral transform (3) to have the form (5).

Considering a Hilbert space of square integrable functions (of one variable, for simplicity) $L^2(R)$ with transitive action of the affine group

$$G: x \to x' = ax + b, \tag{6}$$

$$(ab) \circ (a',b') = (aa',\ ab' + b), \tag{7}$$

we define the representation $U(g)$ as

$$[U(a, b)\,\psi](x) = \frac{1}{\sqrt{a}}\,\psi\left(\frac{x-b}{a}\right) \tag{8}$$

and the left invariant measure in the form

$$d\mu_L(a, b) = \frac{da\,db}{a^2},$$

which follows from (7).

For the case of affine group (6), which is in question in the present paper, it is convenient to evaluate the normalization constant C_ψ, defined by (4) in Fourier representation[2]; the substitution

$$\psi(x) = \frac{1}{\sqrt{2\pi}} \int e^{-i\omega x}\,\tilde{\psi}(\omega)\,d\omega$$

and (8) into (4) after a straightforward calculation gives

$$C_\psi = 2\pi \int \frac{|\tilde{\psi}(\omega)|^2}{|\omega|}\,d\omega < \infty, \tag{9}$$

while the tranform itself has the form:

$$T_\psi(a, b)\,f = C_\psi^{-1/2} \int \frac{1}{\sqrt{|a|}}\,\psi\left(\frac{b-t}{a}\right) f(t)\,dt, \tag{10}$$

$$f(t) = C_\psi^{-1/2} \int\int \frac{1}{\sqrt{|a|}}\,\psi\left(\frac{t-b}{a}\right)[T_\psi(a, b)\,f]\,\frac{da\,db}{a^2}. \tag{11}$$

[2]Here and after the representation $U(a, b)\,\tilde{\psi}(\omega) = \sqrt{|a|}\,\tilde{\psi}(a,\omega)\exp(i\,\omega b)$ is useful to simplify calculations.

3. Basic Properties

The pair of a direct and an inverse wavelet transform (10,11) taken together with the admissibility condition (4) still leaves us considerable freedom in the choice of analysing wavelet ψ. Practically, the admissibility condition (4) taken in the Fourier representation (9) means the vanishing behaviour of $\tilde{\psi}(\omega)$ in the neighbourhood of $\omega = 0$; which can be redundantly satisfied if $\psi(0) = 0$ is implied; the latter, in turn, means

$$\int \psi(t)\, dt = 0. \tag{12}$$

The latter equation provides the insensibility of wavelet transform to a constant shift of the function in question

$$[T_\psi(a, b)](f + \text{const}) = [T_\psi(a, b)]f.$$

The simplest choice of analysing wavelet satisfying the condition (12) is the so-called Haar wavelet:

$$\psi(x) = \begin{cases} 1 & \text{for } 0 < x < 1/2 \\ -1 & \text{for } 1/2 \le x < 1 \\ 0 & \text{elsewhere .} \end{cases}$$

The Haar wavelet, being the simplest one for numeric implementation, has got a lot of applications, mainly in image and signal processing, which we consider later in this paper. The next straightforward generalization of the condition (12) is the vanishing momenta requirement

$$\int dx x^m \psi(x) = 0, \quad \forall m, 0 \le m < n; n \in Z.$$

This requirement gives rise to a family of vanishing momenta Gaussian wavelets [5]

$$g_n(x) = (-1)^{n+1} \frac{d^n}{dx^n} e^{-x^2/2}, \quad n > 0. \tag{13}$$

In Fourier space $\hat{g}_n(\omega) = -(i\omega)^n e^{-\omega^2/2}$ has a zero of order n in $\omega = 0$.

In this family the first two wavelets are most popular: $g_1(x) = -x \exp\left(-\frac{x^2}{2}\right)$, which is antisymmetric and thus suitable for some statistical applications to be considered later, and the Maar wavelet $g_2(x) = (1 - x^2) \exp\left(-\frac{x^2}{2}\right)$, often called the «Mexican hat».

The normalization constant C_{g_n}, which can be easily calculated in the Fourier space, for the family of vanishing momenta wavelets (13) is

$$C_{g_n} = 2\pi(n-1)!$$

Among the other wavelets, the difference of two Gaussians

$$\psi_b(x) = e^{ibx}e^{-x^2/2} = \sqrt{2}\, e^{-b^2/4}e^{ibx}e^{-x^2},$$

considered in the pioneering work [6] should be mentioned.

Another property of wavelet analysis provided by (8), is that a dilated wavelet has the same energy as the original one

$$\int \left| \frac{1}{\sqrt{a}} \psi\left(\frac{t}{a}\right) \right|^2 dt = \int |\psi(t)|^2 dt.$$

Since the energy is conserved under dilatations, wavelet analysis is equally sensitive to the contributions of low and high frequency bands. It is its great advantage, say in comparison to Gabor expansion. The dilatation parameter a here has a plain interpretation: if $\psi(t)$ is a sound recorded on a tape, then $a^{-1/2}\psi(t/a)$ with $a=2$ is the sound obtained by replaying the tape at half speed.

The (global) energy conservation law also holds:

$$\int |f(t)|^2 dt = \int |T_\psi(a,b)f|^2 \frac{da\, db}{a^2}.$$

Among other properties of the wavelet transform we should indicate its property under scale transform:

$$[T_\psi(a,b)]\, f(\lambda t) = \lambda^{-1}[T_\psi(\lambda a, \lambda b)]\, f(t).$$

We should also mention that in numerical implementations the decomposition of a unity

$$\hat{1} C_\psi = \int_G U(g)\,|\psi\rangle\, d\mu_L(g)\, \langle\psi|\, U^*(g),$$

which follows from general formula (5), turns out to be a sum over a discrete frame

$$A\hat{1} \le \sum_j |\psi_j\rangle\langle\psi_j| \le B\hat{1},$$

where $A, B > 0$ are some positive constants. This basis, nonorthogonal and redundant in general, ensures the stability of the wavelet transform: local perturbations of wavelet coefficients cause only local perturbation of the image.

4. Applications to Signal Analysis and Synthesis: First View

As was mentioned in previous section, the dilatation of a wavelet with a factor $a=2$ corresponds to the half speed playback of a tape or to one octave down shifts. Evidently, any musical melody remains recognizable after a global shift by an integer number of octaves. This fact makes the wavelet transform a credible tool in acoustics, speech processing and music.

For practical applications it is convenient to use some particular forms of the integral transforms (10), (11). Here we list these transformations following [6].

1. *Voice transform of f* with respect to ψ is a wavelet transformation (10) taken on the logarithmical scale.

$$(Z_\psi^\pm)[f](b, u) = \frac{2^u}{k_\psi} \int \psi(\pm 2^u (b - t))\, f(t)\, dt, \tag{14}$$

where $k_\psi = \frac{\sqrt{2\pi}}{\ln 2} \cdot \int \frac{\tilde{\psi}(\omega)}{|\omega|} d\omega$. The scale factor 2 is chosen for fast numerical implementation.

The voice transform allows an elegant way to represent inverse formula (11) in the form of an octave series

$$f(t) = \int [(Z_\psi^+ f)(t, u) + (Z_\psi^- f)(t, u)]\, du$$

or $f(t) = \sum_{n=-\infty}^{\infty} f_n^+ + f_n^-$, where $f_n^\pm(t) = \int_n^{n+1} (Z_\psi^\pm f)(t, u)\, du$.

2. Another useful representation, which has some advantages being not expensive in memory space, is known as a *cycle-octave representation*

$$(C_\psi^\pm f)(v, u) = \frac{2^{-u}}{k_\psi} \int \psi\,(\pm (v - 2^u t))\, f(t)\, dt.$$

Practically, instead of basic representation (10), (14) the Fourier representation is often used

$$(T_\psi f)(b, a) = C_\psi^{-1/2} |a|^{1/2} \int e^{i\omega b}\, \tilde{\psi}\,(\omega a)\, \tilde{f}(\omega)\, d\omega \tag{15}$$

and

$$(Z_\psi^\pm f)(b, u) = k_\psi^{-1} \int e^{i\omega b}\, \tilde{\psi}(\pm 2^u\, \omega)\, \tilde{f}(\omega)\, d\omega,$$

respectively. This provides a possibility of using FFT and FFT-like algorithms.

5. Wavelets and Fractals

The best way to study any physical problem with known symmetry is to build a functional basis with the symmetry as close to that of the problem as possible. For this reason a system of spherical functions is the best one to fit the problem with spherical (SO_3) symmetry, while Fourier decomposition is apt to the problems invariant under translations.

The matter turns out to be even more conspicuous when one studies fractals — singular (nondifferentiable) self-similar objects [7]. On the one hand, the invariance under scale transformations (or self-similarity) is the symmetry group the *WT* is based on; on the other, with no requirements of differentiability the wavelet analysis seems to be an ultimate tool to study singular objects. In standard multifractal analysis, the properties of these singular objects are considered in terms of a (singular) measure μ, singularity spectrum of this measure $f(\alpha)$ and the power behaviour of a partition function

$$Z(l, q) = \sum_i (\mu_l)_i^q \sim l^{\tau(q)}; \quad \mu_l(x_0) \sim l^{\alpha(x_0)},$$

where the sum is taken over all disjoint intervals of size l, containing the points of the considered fractal set; $(\mu_l)_i$ is the measure of the i-th interval. The power behaviour of the partition function is characterized by some function $\tau(q)$ related to $f(\alpha)$ and expressed via fractal dimension

$$D_q = \frac{\tau(q)}{q-1}.$$

For a globally self-similar object (monofractal) $D_q = D_0$ does not depend on q

$$\alpha = f(\alpha) = D_q = D_0, \forall_q.$$

To perform wavelet decomposition of a singular measure $\mu(x) = \int_0^x d\mu$ it is convenient to use the vanishing moment wavelet family (13).

The measure $\mu(x)$ can be represented via its wavelet transform

$$\mu(x) = C_g^{-1/2} \int_0^\infty \frac{da\, db}{a^2} \frac{1}{\sqrt{a}} g\left(\frac{x-b}{a}\right) T_g(a, b).$$

An arbitrary function $g(x)$, cannot be used as a basic wavelet — it is required to satisfy the admissibility condition (4). This restriction, however, is rather loose, and allows one to choose a wavelet within a large variety of admissible functions, say from the family (13). This redundancy is undoubtedly of great benefit for the analysis of fractal structure. It provides us with a powerful mathematical microscope with magnification a^{-1} and dispensable optics labelled by n.

To illustrate this, we can consider the «devil's staircase» — a singular measure of the triadic Cantor set shown in Fig.1. The maxima of its wavelet transform $T_g(a, x)\,\mu$, shown in Fig.2, exactly resemble the structure of the original set.

Besides the graphic facilities, a number of useful theorems provide a basis for analytical studies of fractal objects via wavelets. Roughly speaking, the analytical treatment is based on the fact that the collection of all wavelet transform maxima contains complete information on the measure in question.

Some useful results are listed below:

- **Theorem 2** (*Holshneider*, [8]). *Let* μ *be a bounded locally integrable function such that*

$$\mu(x) - \mu(x_0) = 0(|x - x_0|^h), \quad h \in [0, 1]$$

then

$$T_g(a, x) = O(a^{h+1/2}) \tag{16}$$

inside the cone $|x - x_0| \le \text{const}$.

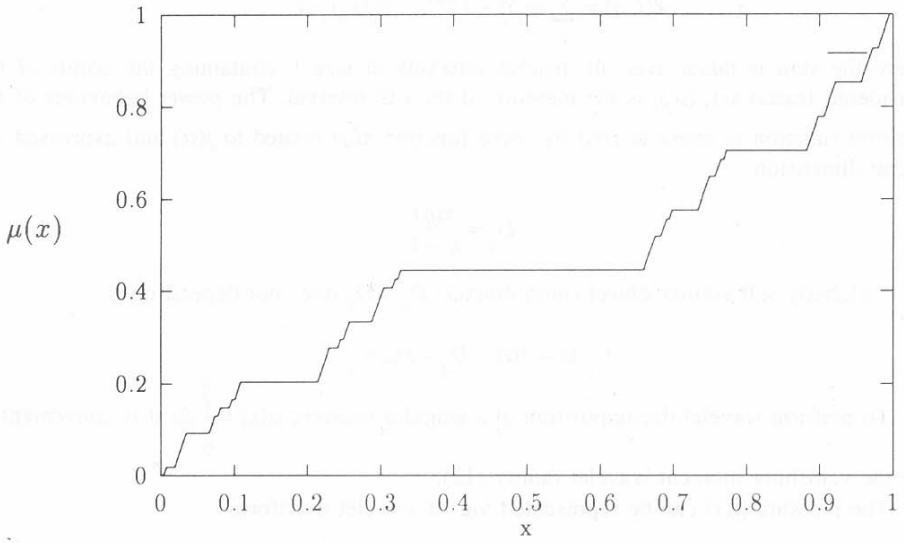

Fig.1. «Devil's staircase» — a singular measure of the triadic Cantor set

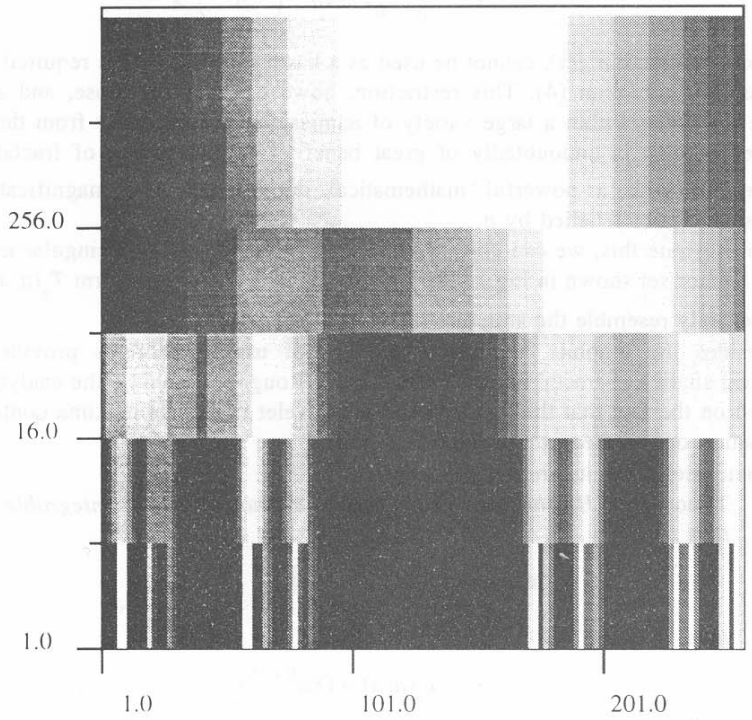

Fig.2. Wavelet coefficients for a «devil's staircase» taken with g_1-wavelet

- The partition function can be constructed directly on the set of wavelet coefficients:

$$Z(a, q) = \sum_{\text{over all maxima: } \{x, (a)\}} |T_g(a, x)|^q.$$

The power behaviour of the measure can be derived from this equation like free energy in thermodynamics $\tau(q) = \lim_{a \to 0} \frac{\ln Z(a, q)}{\ln a}$.

6. Wavelets in Biology

The analysis of DNA sequences is one of the principal branches of modern cellular biology. It was shown in a number of recent studies that the distribution of nucleotides *A*, *T*, *C*, *G* in a real DNA chain is a fractal one. Thus, the fractal and multifractal tools can be applied. Wavelet analysis is an indispensible tool in this relation.

In general, the occurrence of a certain nucleotide in a certain position of the DNA chain, labeled by a length parameter l, can be described as a random process $X(l, \cdot)$. Thus, for the case of the above-mentioned 4-letter alphabet, we deal with a probability space $(\Omega, \mathcal{U}, P)$, with $\Omega = \{A, T, C, G\}$ and a family of four random processes

$$X_z = \{X_z(l, \omega); l \in R, \omega \in \Omega\},$$

such that

$$X_z(l, \omega) = \begin{cases} 1 & \text{if } \omega = z \\ 0 & \text{otherwise.} \end{cases}$$

Instead of calculating correlations, as was done in [9], we proceed with the integral measures

$$\mu_z(s) = \int_0^s X_z(l, \omega)\, dP(\omega)\, dl \equiv \int_0^s d\mu_z, \tag{17}$$

which count the total number of each of the nucleotides $z = A, T, C, G$ up to the l-th position in the chain.

Since the measures in question (17) are supposed to be generally nondifferentiable, we first have to study their scaling behavior $\mu(x) - \mu(x_0) \approx |x - x_0|^h$.

The extraction of the Lipschitz—Hölder exponent h from the experimentally obtained measure is a typical problem in physics of fractals, in DNA study this was performed in the same way, using the scaling theorem [8] for the function $\mu(l)$ (see eq.16). The details of the method can be found in [10]; hereafter we present the main results obtained in [10] with the help of the g_2-wavelet.

For the DNA sequence of Chinese Hamster cells [11] with the length of 11838 nucleotides the middle-data section of wavelet coefficients gives the scaling exponents h.

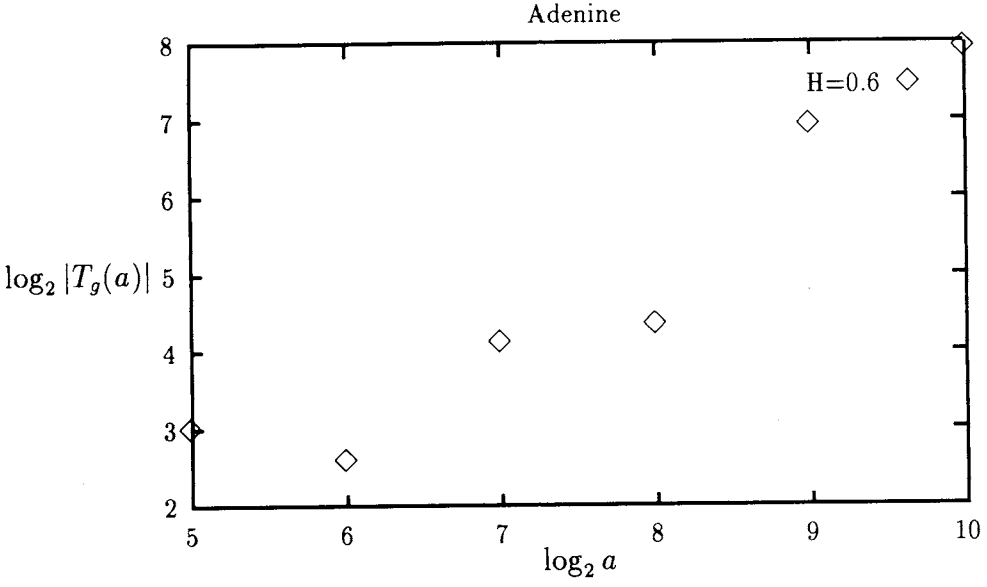

Fig.3

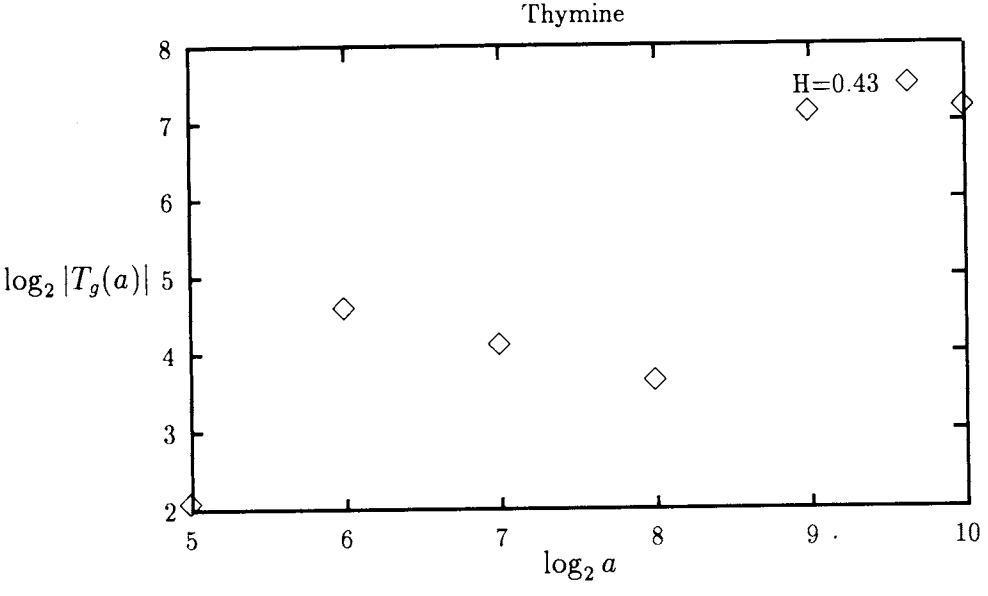

Fig.4

Figs.3—6. The dependence of (binary logarithms of) g_1-wavelet coefficients for the measure functions taken at the middle of the data for the adenine, thymine, cytosine and guanine, respectively. The values of the Lipschitz–Hölder exponents presented in the pictures were obtained with the best line approximation

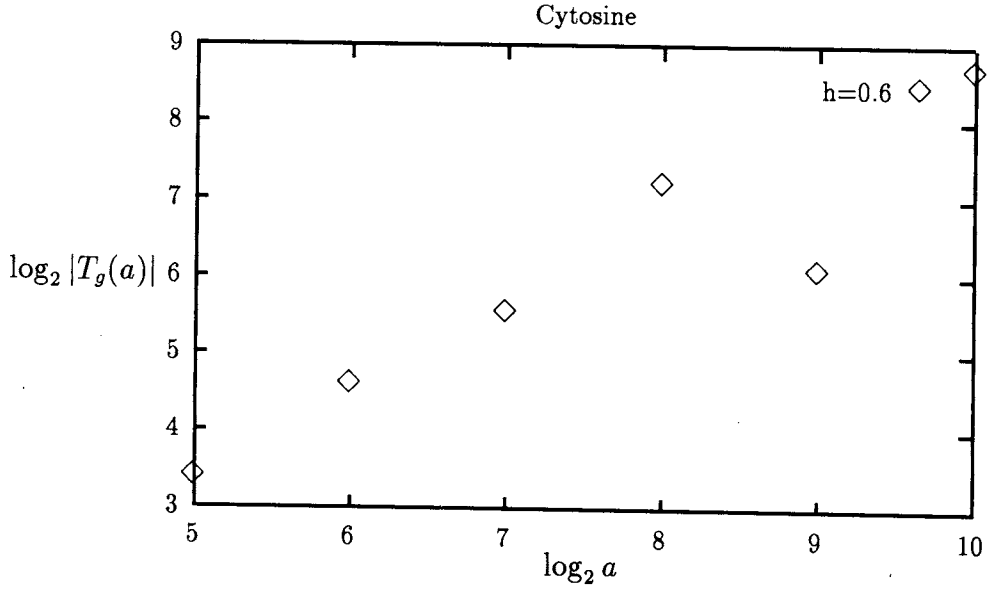

Fig.5

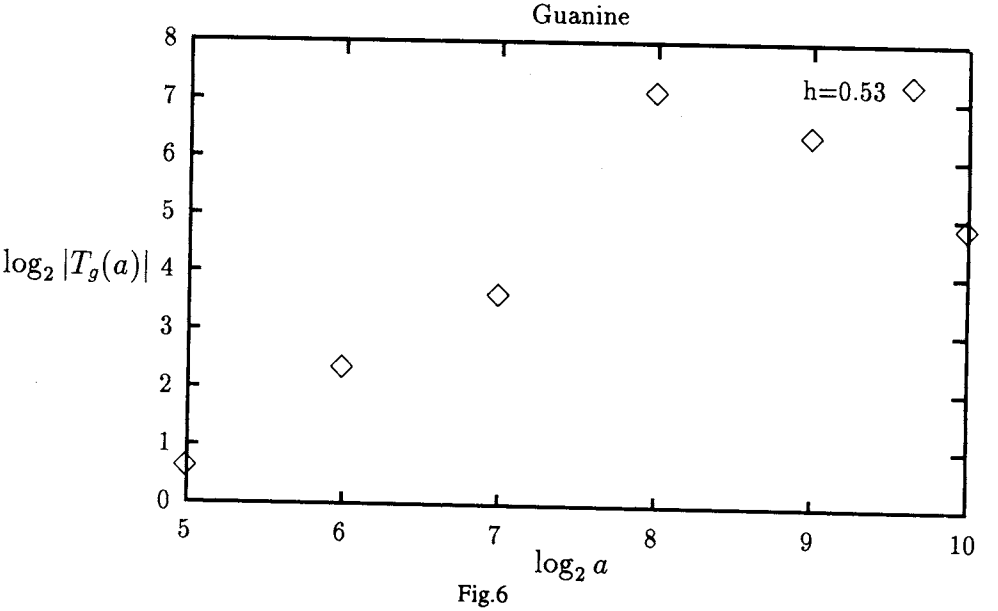

Fig.6

The logarithmic plots $\log_2 |T_g(a, x)|$ for the measures μ_a, μ_t, μ_c, μ_g are presented in Figs.3—6. The plots were obtained at the middle of the range, $x_m = 4096$; however the behaviour of the sections at other points is not seriously different. The corresponding Lipschitz-Hölder exponents are presented in the table.

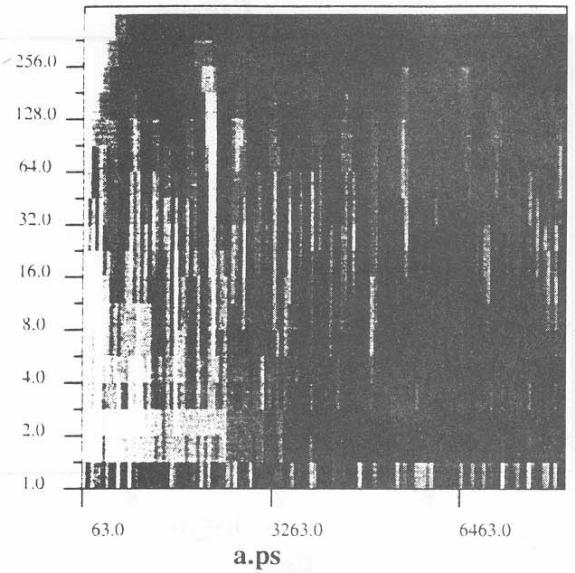

Fig.7

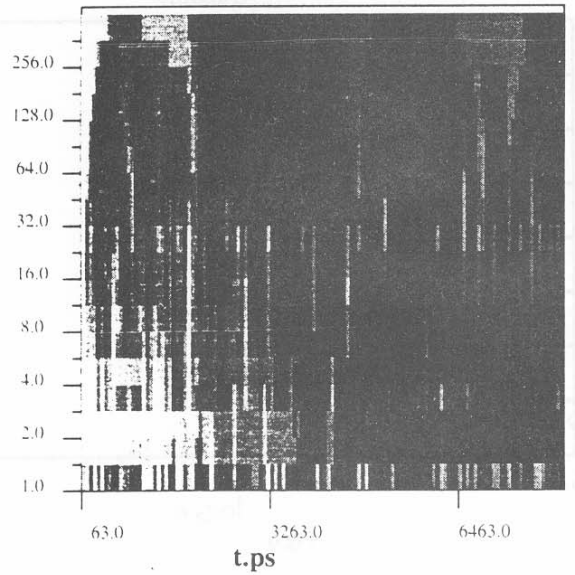

Fig.8

Figs.7—10. The grey density plots of wavelet coefficients (up to 2^{10} power scale) for the adenine, thymine, cytosine and guanine, respectively. The fragmentation processes clearly distinguish at 2^6, 2^7 and 2^9 scales

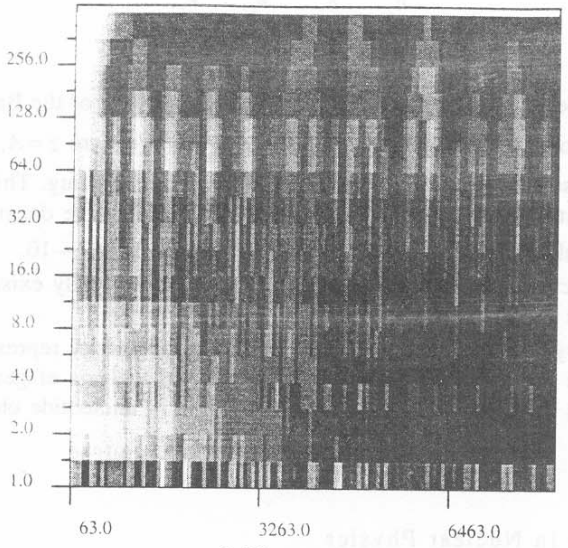
256.0
128.0
64.0
32.0
16.0
8.0
4.0
2.0
1.0
63.0
3263.0
6463.0
c.ps

Fig.9

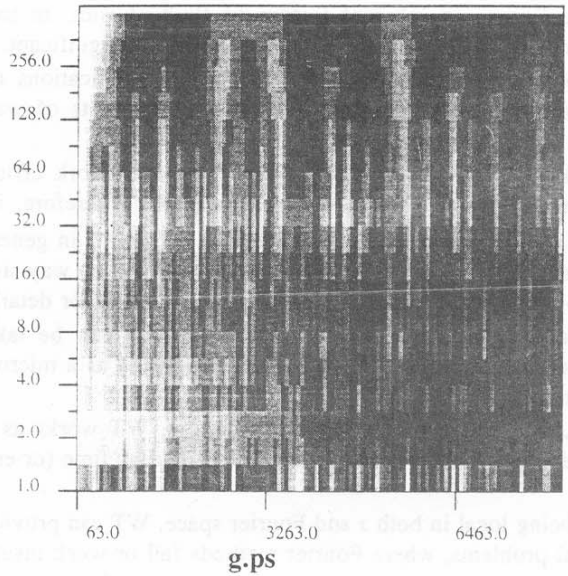
256.0
128.0
64.0
32.0
16.0
8.0
4.0
2.0
1.0
63.0
3263.0
6463.0
g.ps

Fig.10

h_A	h_T	h_C	h_G
0.60	0.43	0.60	0.53.

These coefficients are conspicuously close to the $h_B = 1/2$ of the Brownian motion, the purely random process. However, the difference $h_z - h_B$, where $z = A, T, C, G$, which has the magnitude of several per cent, cannot be regarded as vanishing. This difference can be caused by branching processes which can be clearly seen in the density plots of wavelet coefficients, at scale approximately equal to 2^7 or 2^8, see Figs.7—10.

Thus, we conclude that the scaling in DNA chains does really exist. This scaling is of multifractal nature (see, e.g., [11]) rather than global one.

As an auxiliary result, we can mention that the color-density representation of wavelet coefficients which proved to be a powerful tool for the analysis of general fractals seems to be of great use for identifying branching processes in nucleotide chains as a computer graphic tool.

7. Wavelets in Nuclear Physics

Up to now the most common applications of WT belonged to either turbulence data analysis, where scaling is an inherent feature of fluid physics, or to image processing, where the singularity detection and local reconstruction are significant.

Recently a lot of interest was attracted to possible applications of wavelets in both theoretical and experimental nuclear physics. The main merits of wavelets valuable for experimental data processing are:

- Firstly, since the works of Zimin, WT proved to work efficiently in situations where cascade processes play a significant role. Therefore, if the measure $\mu(x)$ describes an event number at a certain point x, ($x \in R^3$ in general), then the search for *jet* events can be performed with the aid of WT, in a way similar to the «devil's staircase» singularity reconstruction (See, e.g., [7,10] for details).
- In the simplest one-dimensional case, $x \in [0, 2\pi]$ can be taken for the angular coordinate of the detector; the WT can be regarded as a microscope with variable angle resolution.
- Secondly, if x is regarded as time (or energy), WT works as a tool for studying time (or energy) scaling of the process described by time (or energy) event density $\mu(x)$.
- Thirdly, being local in both x and Fourier space, WT can provide more information in spectral problems, where Fourier methods fail or work insufficiently.
- The contributions of different frequency bands to WT are kept reasonable separated. This separation is achieved with quite insignificant loss of resolution in time variable (if a signal is considered). That's why the reconstruction is «robust» in the sense of being stable under small perturbations, which enables one to distinguish between «useful» low bands (in Fourier space) and contributions of close high frequencies $\omega_1 - \omega_2 \approx 0$ usually generated by noise.

From the theoretical point of view the possible applications of wavelets are even more appealing, since the wavelet transform is based on the scaling symmetry — one of the most important symmetries in physics. Here we mention a few facts related to self-similarity which could be studied with the help of wavelets [12]:

- *Local Parton Hadron Duality* [13], i.e., the similarity between momentum spectra of hadrons and those of partons. This similarity, which is closely related to n-parton correlations and multiplicity moments behaviour in phase space, has been studied in [14].
- The fractal behaviour of final multiparton states [16] was studied by several authors. They calculated the fractal dimension directly from multiplicity distribution moments and study the entropy of secondary particles

$$S = -\sum_n P_n \ln P_n ,$$

where P_n is the probability of having «n» produced particles in the final state [17]. They found the scaling behaviour, but, as the method was rather rough (see [7] for the shortcomings of the fractal dimension calculations without wavelets), rare, but interesting events could be lost.

- Recently, fractal analysis of multiparticle production in hadron-hadron collisions has been done by other authors [15].

All these studies evidently admit the application of wavelet transform. Recently, the wavelet transform as an image processing method was also applied to separation of secondary particles (K-mesons, in particular) in d + Au interactions. Following [12], here we describe the method and results.

7.1. Secondary Particle Separation as an Image Recognition Problem

7.1.1. Problem. The wavelet method has been applied to the processing of time-of-flight vs. energy data plots obtained from d + Au → ... — reactions in experiments carried out at the Nuclotron using the internal target at a deuteron momentum of 3.8 GeV/c in March 1994.

In Fig.12 the mass spectrum of the primary data obtained by standard method of comparing the time of flight and the energy

$$\beta = \frac{v}{c} = \frac{l}{tc} = \sqrt{\frac{E^2 - m^2}{E^2}} \qquad (18)$$

is presented.

Due to the presence of both π-mesons and protons ($E \sim 250$ MeV), which dominate in the central region of the E vs. TOF plot, Fig.11, it is difficult to distinguish other events in this region. Besides, high energy protons ($E > 400$ MeV) due to decreasing energy loss give a contribution mainly to the low energy region about 200 MeV.

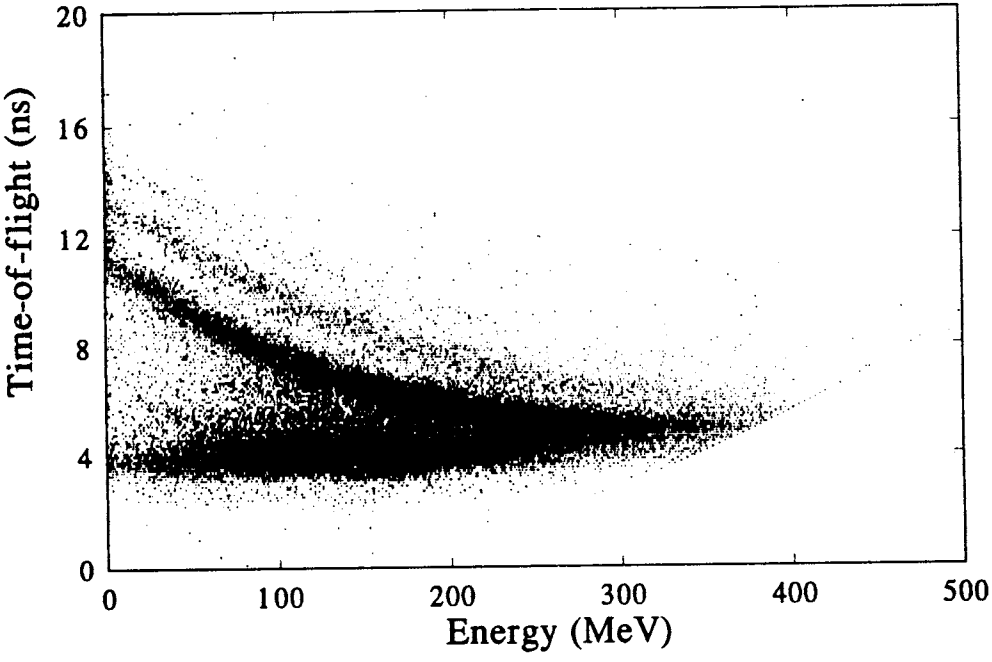

Fig.11. E vs. TOF plot of primary experimental data

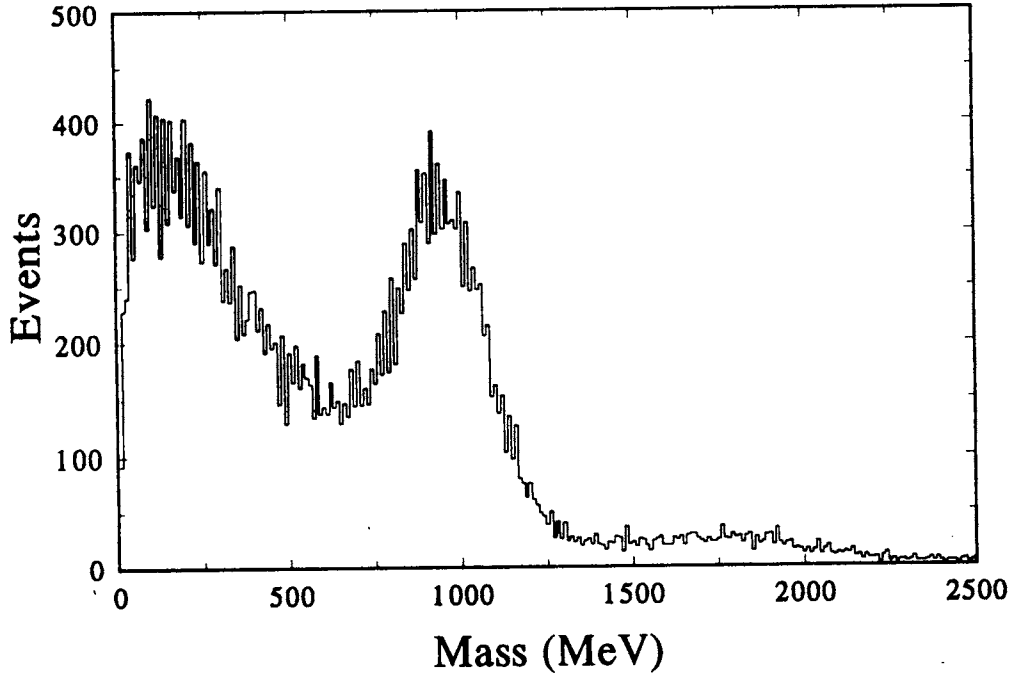

Fig.12. Spectrum of reconstructed mass obtained from primary data

7.1.2. Algorithm. The main idea of implying a wavelet analysis to investigation of events in nuclear and high energy physics is to use its good properties in separating events from noise. Using wavelet one can look at experimental data with various resolution. This can be used to search for tracks of particles and different kinds of events, etc.

To use a multiresolution analysis [18] one should choose a family of closed subspaces $V_m \subset L^2(R)$, $m \in Z$, such that

1. $f(x) \in V_m \Leftrightarrow f(2*x) \in V_{m-1}$

2. $\ldots \subset V_2 \subset V_1 \subset V_0 \subset V_{-1} \subset V_{-2} \subset \ldots$,

$\cap V_m = 0, \quad \cup V_m = L^2(R)$

3. there is a $\varphi \in V_0$ such that its linear integer translations $\varphi_n^0(x) = \varphi(x+n)$ constitute a basis in V_0 (consequently, functions φ_n^m constitute a basis in V_m),

4. there exist $0 < A \le B < \infty$, such that for all $(c_n)_{n \in Z} \in l^2(Z)$,

$$A \sum_n |c_n|^2 \le \| \sum_n c_n \varphi_n^m \|^2 \le B \sum_n |c_n|^2.$$

The orthogonal projections of a function which we analyse on a chain of subspaces V_m represent snapshots of this function with different resolution. Choosing an appropriate basic function φ, one could select different kinds of snapshots.

To make the decomposition close, one should also define a chain of subspaces W_m orthogonal to V_m, such that

$$V_{m-1} = V_m \oplus W_m . \tag{19}$$

The coefficients of a projection on V_m and W_n are

$$s_n^m = \int f(x)\, \varphi_n^m(x)\, dx, \quad d_n^m = \int f(x)\, \psi_n^m(x)\, dx, \tag{20}$$

where in a discrete case a sum is implied. For the simplest case of the Haar wavelet the basic functions are:

$$\varphi_k^j(x) = \begin{cases} |I_k^j|^{-1/2} & \text{for } x \in I_{j,k} \\ 0 & \text{elsewhere,} \end{cases} \tag{21}$$

$$\psi_k^j(x) = \begin{cases} 2^{-j/2} & \text{for } 2^j(k-1) < x < 2^j(k-1/2), \\ -2^{-j/2} & \text{for } 2^j(k-1/2) \le x < 2^j k, \\ 0 & \text{elsewhere} \end{cases} \tag{22}$$

I_k^j denotes the supporter of j-th level basic functions

$$I_j \equiv I_k^j = [2^j(k-1),\, 2^j k].$$

The approximate reconstruction formula has the form

$$P_m f = \sum_n s_n^m \varphi_n^m + \sum_n d_n^m \psi_n^m . \tag{23}$$

In our two-dimensional problem we used a pyramidal scheme with a basis taken in the form of a tensor product

$$h_{I\times J} = (\psi_I \oplus \varphi_I) \otimes (\psi_J \oplus \varphi_J),$$

or explicitly, $\{h_1, h_2, h_3\} = \{\psi_I(x)\,\psi_I(y), \psi_I(x)\,\varphi_I(y), \varphi_I(x)\,\psi_I(y)\}$. The corresponding coefficients can be easily derived from formulae (20):

$$\begin{aligned}
s^{j+1}_{k_x,k_y} &\sim s^j_{2k_x-1,\,2k_y-1} + s^j_{2k_x-1,\,2k_y} + s^j_{2k_x,\,2k_y-1} + s^j_{2k_x,\,2k_y}\\
d^{j+1}_{(1);\,k_x,k_y} &\sim s^j_{2k_x-1,\,2k_y-1} - s^j_{2k_x-1,\,2k_y} - s^j_{2k_x,\,2k_y-1} - s^j_{2k_x,\,2k_y}\\
d^{j+1}_{(2);\,k_x,k_y} &\sim s^j_{2k_x-1,\,2k_y-1} - s^j_{2k_x,\,2k_y-1} + s^j_{2k_x-1,\,2k_y} - s^j_{2k_x,\,2k_y}\\
d^{j+1}_{(3);\,k_x,k_y} &\sim s^j_{2k_x-1,\,2k_y-1} + s^j_{2k_x,\,2k_y-1} - s^j_{2k_x-1,\,2k_y} - s^j_{2k_x,\,2k_y},
\end{aligned}$$

where s^0 stand for the primary data.

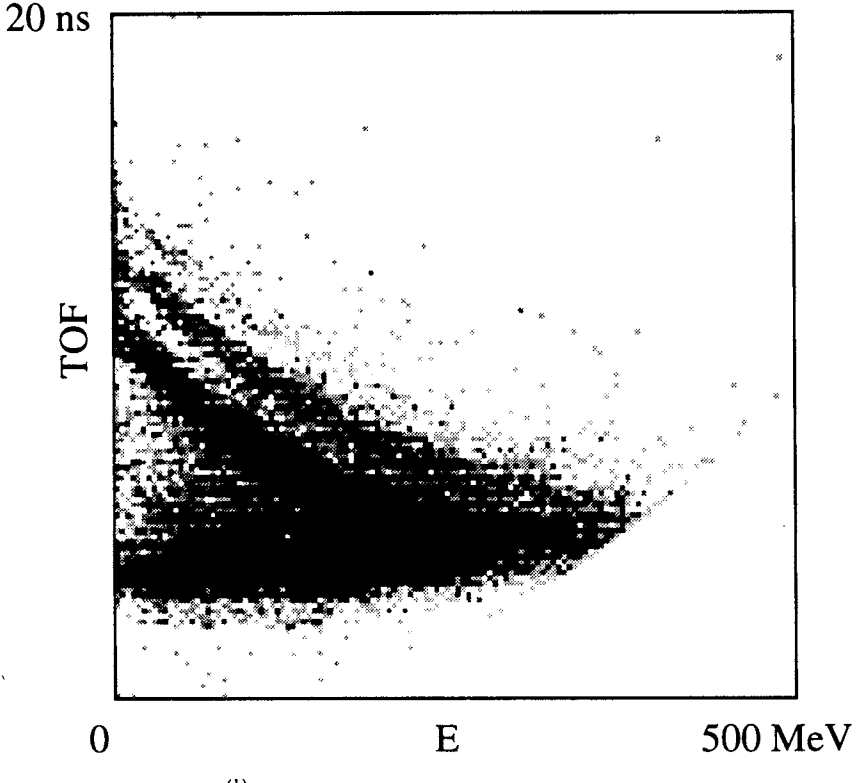

Fig.13. $s^{(1)}$ coefficients plot for the data set of Fig.11

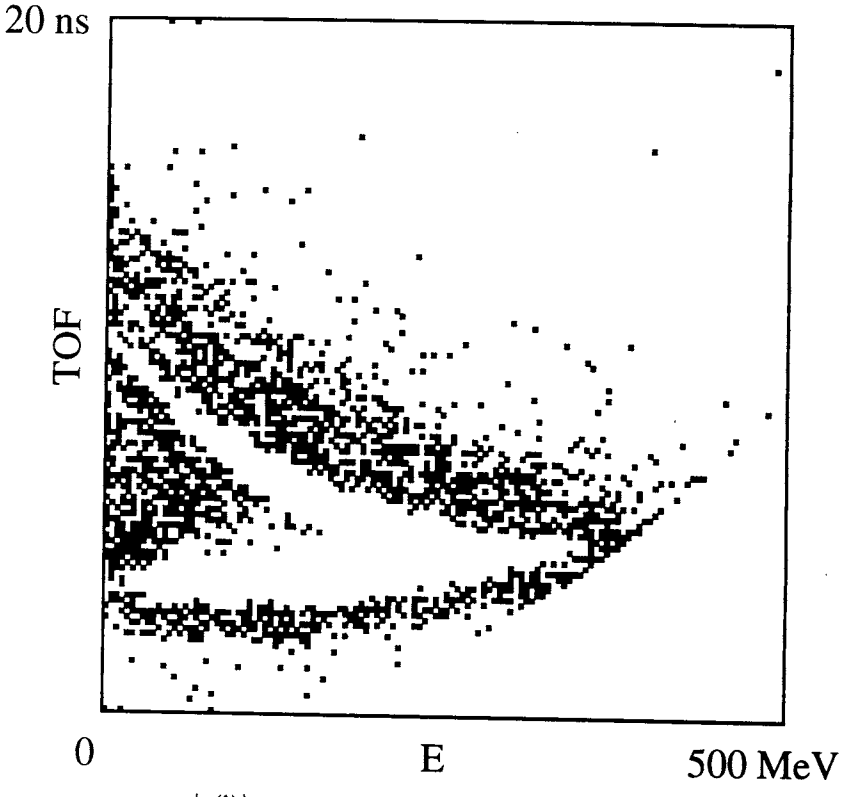

Fig.14. $|d^{(1)}|$ coefficients plot for the data set of Fig.11

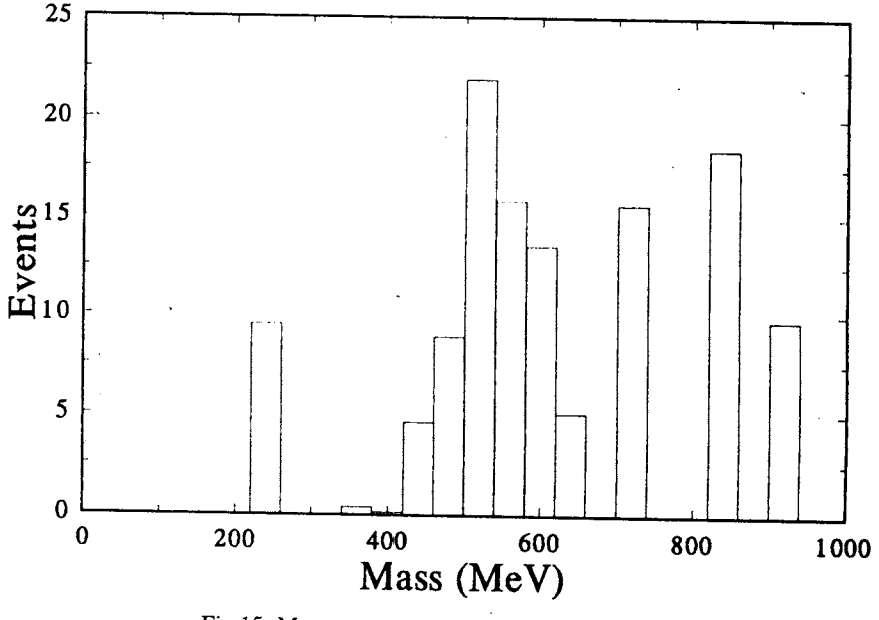

Fig.15. Mass spectrum obtained after filtering

7.1.3. Results. The primary data E—dt—plot is shown in Fig.11. The X-axis corresponds to ADC channel numbers, Y-axis to TDC ones. (Both axes are scaled by factor 4). In this plot, against a noisy background we can distinguish two contrast regions: the upper one, which corresponds to secondary protons, and the lower one, which corresponds to π-mesons.

To clear out the contribution of the dominating processes we performed the wavelet analysis. Having calculated the wavelet image (the Haar wavelet was used) of the initial data plot we substracted the central domain, in which $d^{(2)}$ coefficients (See Fig.14) practically vanish.

The resulting mass spectrum is presented in Fig.15. We identify the central peak near 500 MeV, clearly distinguished in mass histogram,with the K-meson contribution.

Besides, sequentially scaling the picture, we can clearly distinguish 4 regions:

- upper right region: secondary deuterons
- two above-mentioned regions
- a K-meson branch.

7.2. Fitting Distributions with Wavelets

7.2.1. Problem. A typical problem of experimental nuclear physics is that of separating several Gaussians which contribute to the same experimentally obtained spectrum. Usually, to cope with this problem, some parametric methods evolving numerical minimization are used. Wavelet decomposition provides a nonparametric method to separate the contributions of several Gaussians [20].

Let us consider an approximation of an experimental data distribution, e.g., a number of particles per channel vs. energy, by the sum of finite number of Gaussian sources

$$f_{\exp}(x) = \sum_k \frac{N_k}{\sqrt{2\pi\sigma_k^2}} \exp\left(-\frac{(x - x_m^k)^2}{2\sigma_k^2} \right), \tag{24}$$

where $\sum_k N_k = N$ is the total number of registered particles.

If we suppose that $f_{\exp}(x)$ is a square-integrable function, the solution of the equation

$$f_{\exp}(x) - \sum_k \frac{N_k}{\sqrt{2\pi\sigma_k^2}} \exp\left(-\frac{(x - x_m^k)^2}{2\sigma_k^2} \right) = 0$$

can be found analytically. Let us start with a single gauss distribution

$$f_{\text{gauss}}(x) = \frac{N}{\sqrt{2\pi\sigma_k^2}} \exp\left(-\frac{x^2}{2\sigma_k^2} \right), \tag{25}$$

where, without loss of generality, we set $x_m^1 = \bar{x} = 0$.

Instead of calculating different moments of the probability distribution we perform wavelet decomposition of the spectrum in question. Since we are going to analyse Gauss distributions, it is natural to choose the analysing function g — the basic wavelet — from the family of vanishing momenta wavelets (13).

It should be mentioned, that $g_0(x)$ does not fit the problem, since $c_{g_o} = \infty$ and the inverse transform (11) is not defined for this case. This fact hints that the direct decomposition of $f_{\exp}$ into the sum of Gaussians is not unique, and hence the problem requires more general system of basic functions.

Prior to study distribution functions with the family of wavelets (13), let us recall some useful formulae

1. The Fourier transform of the g_n family is

$$\tilde{g}_n(k) = -(ik)^n e^{-k^2/2}.$$

2. We can define a formal generating function for the wavelet family g_n

$$\tilde{g}(s, k) = \exp(iks - k^2/2), \tag{26}$$

such that

$$\tilde{g}_n(k) = -\left(\frac{d}{ds}\right)^n \tilde{g}(s, k)\Big|_{s=0}. \tag{27}$$

For a single Gaussian distribution (25), to calculate the convolution (10) for an arbitrary basic function from the family g_n we use the generation function (26):

$$(T_{g_n} f_{\text{gauss}})(a, b) = -\left(\frac{d}{ds}\right)^n (T_{g_s} f_{\text{gauss}})(a, b)\Big|_{s=0}, \tag{28}$$

where g_s stands for $g(s, \cdot)$. Substituting (15) into the latter equation, we obtain

$$(T_{g_s} g_{\text{gauss}})(a, b) = N\sqrt{\frac{a}{2\pi c_{g_s}}} \int dk \exp\left(ik(b + as) - \frac{k^2}{2}(a^2 + \sigma^2)\right) =$$

$$= N\sqrt{\frac{a}{c_{g_s}}} \frac{\exp\left(-\dfrac{(b + as)^2}{2(a^2 + \sigma^2)}\right)}{\sqrt{a^2 + \sigma^2}}. \tag{29}$$

The formal normalization constant c_{g_s} should be replaced by concrete c_{g_n} after taking the derivatives.

7.2.2. Single Source Distribution. The simplest way to find the distribution parameters for the case of a single Gaussian source is to use the coefficients of its g_2 decomposition. Eq. (29) for $n = 2$ leads to

$$(T_{g_2} f_{\text{gauss}})(a, b) = N\sqrt{\frac{a^2}{2\pi}}\left(\frac{a}{a^2+\sigma^2}\right)^{3/2}\left[1-\frac{b^2}{a^2+\sigma^2}\right]\exp\left(-\frac{b^2}{2(a^2+\sigma^2)}\right). \quad (30)$$

Taking the derivative ∂/∂_a of equation (30) at the central point $b=0$ we find the extremum of the g_2 coefficient at a scale

$$a_m = \sqrt{5}\sigma. \quad (31)$$

The value of wavelet coefficient at the extremal point is

$$(T_{g_2} f_{\text{gauss}})(a_m, 0) = \frac{N}{\sqrt{2\pi}\sigma} 5^{5/4} 6^{-3/2} = \frac{N}{\sqrt{2\pi a_m}}\left(\frac{5}{6}\right)^{3/2}. \quad (32)$$

Thus, performing the convolution (10) numerically and finding the maximum of the g_2 wavelet coefficient we obtain the dispersion and amplitude of original distribution.

7.2.3. The Distribution with Two Sources. If the distribution is a sum of two Gaussians and the localization at least of one of them is known, we can find the other with the help of g_1 wavelet.

Without loss of generality we write the analysed function in the form

$$f(x) = \frac{N_0}{\sqrt{2\pi\sigma_0^2}}\exp\left(-\frac{x^2}{2\sigma_0^2}\right) + \frac{N_1}{\sqrt{2\pi\sigma_1^2}}\exp\left(-\frac{(x-x_m)^2)}{2\sigma_1^2}\right). \quad (33)$$

Let us consider the g_1-wavelet coefficient at $x=0$. Since the first term of r.h.s. of (33) is symmetric, whether $g_1(x)$ is antisymmetric under the reflection $x \to -x$, the coefficient $(T_{g_1} f)(a, 0)$ depends on the second term of (33) only.

Explicitly,

$$(T_{g_1} f)(a, 0) = N_1 \frac{x_m}{\sqrt{2\pi}}\left(\frac{a}{a^2+\sigma_1^2}\right)^{3/2}\exp\left(-\frac{x_m^2}{2(a^2+\sigma_1^2)}\right). \quad (34)$$

Thus, knowing $(T_{g_1} f)(a, 0)$ we can determine N_1, σ_1, x_m.

The transformation with the g_1 basic wavelet is practically useful when we are looking for a Gaussian distribution with a center located apart from a certain point x_0. In this case, since $g_1(x)$ is antisymmetric, the local Gaussian fluctuations located at x_0 give no contribution to $(T_{g_1} f)(a, x_0)$. The extremal condition with respect to the scale variable a

$$\frac{\partial(T_{g_1} f)(a, 0)}{\partial a} = 0,$$

can be easily derived from (34), where $x_0 = 0$ without loss of generality. This leads to the biquadratic equation

$$3a^4 - 2x^2a^2 - 3\sigma^2 = 0,$$

which has a real positive solution

$$a_{\text{extr}} = x\sqrt{\frac{1+\sqrt{1+9(\sigma/x)^4}}{3}}. \tag{35}$$

7.2.4. Practical Application. Practically, the method was applied to test the energy spectrum of plastic scintillators produced in Dubna for the NEMO experiment [21]. The electron energy resolution was measured with radioactive source ^{207}Bi emitting 569 keV and 1063 keV γ-quanta and the corresponding internal conversion (K) electrons with the energy 481 keV and 978 keV.

A typical data sample, produced by a standard source with the coincidence measure method, is shown in Fig.16. The spectrum (the total intensity) contains the contributions of K, L, M, N electron lines, and an unknown background.

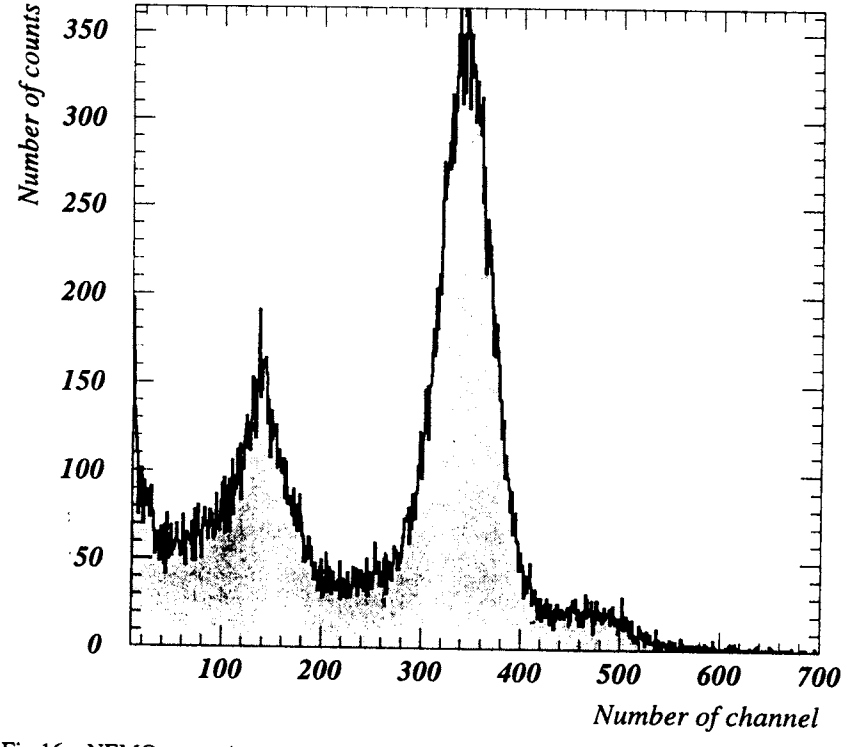

Fig.16. NEMO experiment. The electron energy spectrum registered in plastic scintillator test

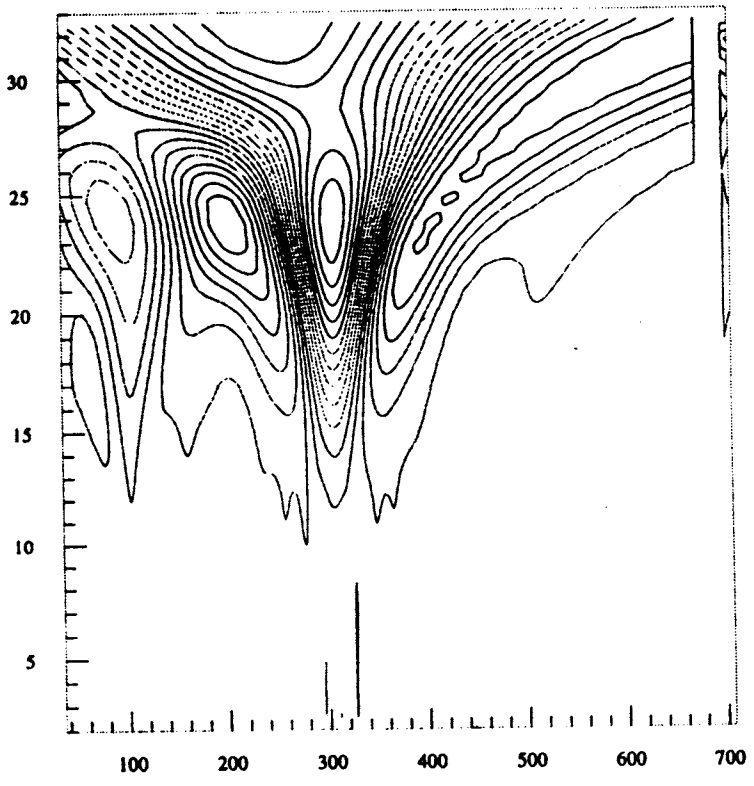

Fig.17. q_2 wavelet coefficient for the energy spectrum

Visualizing the wavelet image of the raw data we obtain a clear picture of the whole process with distinguished local maxima on the scale-versus-coordinate plane. For sufficiently distinguished peaks relation (31) provides a direct method of calculating without any numerical fit. For more complicated noisy data the method provides visualization of local maxima — possible sources of Gaussian distributions. The main advantage of wavelets, appearing even for the case of visually unseparable Gaussian peaks, is that we can see the same picture at different scales simultaneously and look for the sources according to the scale behaviour of wavelet coefficients. Besides, using two different wavelets, symmetric and antisymmetric, say g_2 and g_1, we can make a recurrent procedure based on formulae (32,34).

The plot of the wavelet image of these data is shown in Fig.17. The X-axis corresponds to the electron energy (in channels); the Y-axis corresponds to the $2^{1/4}$ based scale.

All the local maxima can be clearly seen on the plots. For the sufficiently separated peaks the energetic resolution (σ) of the peak can be directly determined from equation (31).

Since the statistics is not high enough, it requires both experimental knowledge and efficient data processing methods to get statistically valuable results from the existing data.

8. Conclusion

Wavelet analysis, which has been proved to be an efficient tool in all kinds of signal processing, seems to be even more promising in nuclear physics. There are several reasons for that:

- Being a robust integral transform, wavelet analysis does not require differentiability of the function in question and is stable under local perturbations. That is why it directly (without any preliminary smoothing) provides information about singularities and self-similarity, if they are present in experimental data.
- It is natural to define wavelet transform directly on probability space (and consider differentiable functions as a particular case) — thus we have a nonparametric statistical method [22].
- Wavelet analysis can be used in theoretical nuclear physics and provides a self-similar basis in Hilbert space of state vectors [23]. Thus we have a new bridge between observed statistical properties of quantum systems and their immanent quantum properties.

Acknowledgement

The author is thankful to professor E.B.Zhidkov for stimulating discusion and to Mrs.Y.Padma, the secretary of B.M.Birla Science Centre (India), for typing some parts of this manuscript.

References

1. Gabor D. — Journal of IEE, 1946, 93, p.429.
2. Morlet J. — In: Proc. 51st Annu. Meet. Soc. Explor. Geophys., Los-Angeles, 1981; Zimin V.D. — Izv. Atmos. Ocean. Phys., 1981, 17, p.941.
3. Grossman A., Paul T. — In: Lecture Notes in Physics, vol.211, Springer, Berlin, 1984; Grossman A., Morlet J., Paul T. — J. Math. Phys., 1985, 27, p.2473; Grossman A., Morlet J., Paul T. — Ann. Inst. H.Poincare, 1986, 45, p.293.
4. Carey A.L. — Bull. Austr. Math. Soc., 1976, 15, p.1; Duflo M., Moore C.C. — J. Func. Anal., 1976, 21, p.209.
5. Combes J.M., Grossmann A., Tchamitchan P. — Eds., Wavelets, Springer, Berlin, 1988.
6. Goupillaud P., Grossman A.; Morlet J. — Geoexploration, 1984/85, 23, p.85.
7. Muzy J.F., Bacry E., Arneodo A. — Phys. Rev. Lett., 1991, 67, p.3515; Muzy J.F. et al. — Phys. Rev., 1993, E47, p.875.
8. Holshneider M., Tchamitchan P. — In: Les Ondeletes, ed. by Lemarie P.G., Springer, Berlin, 1990.
9. Peng C.-K. et al. — Nature, 1992, 356, p.168; Voss R.F. — Phys. Rev. Lett., 1992, 25, p.3805.

10. Altaiski M., Mornev O., Polozov R. — B.M.Birla Science Centre Technical Report BSC-CAMCS-95-06-2, To appear in Genetic Analysis: Techniques and Applications.
11. Gale J.M. et al. — J. Mol. Biol., 1992, 224, p.343.
12. Afanasiev S.V., Altaisky M.V., Zhestkov Yu.G. — Nuovo Cim., 1995, A108, p.919.
13. Azimov Ya.I., Dokshitzer Yu.L., Khoze V.A., Troyan S.I. — Z. Phys., 1985, 27, p.65; ibid, 1986, C31, p.231.
14. Ochs W., Wosiek J. — Phys. Lett., 1993, B305, p.144.
15. Boca G., a.o. — Nuovo Cim., 1992, A105, p.865.
16. Gustafson G., Nilson A. — Z. Phys., 1991, C52, p.533.
17. Mikhopadhyay A., Jain P.L., Singh G. — Phys. Rev., 1993, C47, p.410.
18. Daubechies I. — Comm. Pure. Apl. Math., 1988, 16, p.909.
19. Beylkin G., Cifman R., Rokhlin V. — Comm. Pure. Apl. Math., 1991, 44, p.141.
20. Altaiski M., Kochetov O., Kovalenko V. — To appear in Engineering Simulation.
21. NEMO collaboration. — Nuclear Instruments and Methods in Physics Research, 1995, A354, p.338.
22. Frazier M.W. — In: Wavelets: Mathematics and Application, ed. by Benedetto J.J., CRC Press Inc, 1994.
23. Kaiser G. — Phys. Lett., 1992, A168, p.28.
Altaisky M.V. — Preprint ICTP, IC/94/281, Trieste, 1994.

Received on November 28, 1995.